European Journal of Soil Science, June 1998, **49**, 213–229

Integrating properties of soil map delineations into ordinary kriging

G. BOUCNEAU[a], M. VAN MEIRVENNE[a], O. THAS[b] & G. HOFMAN[a]
[a]*Department of Soil Management and Soil Care and* [b]*Department of Applied Mathematics, Biometrics and Process Control, University of Gent, Coupure 653, 9000 Gent, Belgium*

Summary

Stratification of a region based on soil map delineations followed by within-stratum interpolation is sometimes used to combine soil maps and spatial interpolation. However, not all delineations are equally suitable to subdivide an area into precisely located mutually exclusive strata. This paper proposes a flow-path to characterize the nature of soil map delineations and a methodology to integrate the properties of map delineations into ordinary kriging.

Four types of delineations were distinguished based on three criteria: the nature of transition (discontinuous or gradual), the mapping accuracy, and the structure of the within-unit spatial variation. For each type of delineation the ordinary kriging algorithm was modified to integrate its properties in the interpolation.

As a test case, the sand content of the topsoil in the province of West-Flanders (Belgium) was mapped, using independent test data for validation. Inside the mapping units and at delineations identified as gradual transitions, our procedure, termed ordinary kriging integrating properties of map delineations (OKPD), performed similarly to stratified ordinary kriging (SOK). However, close to the delineations identified as inaccurately mapped discontinuities the mean square prediction error of OKPD was 0.64 times that of SOK. Moreover, near these delineations, the prediction variance was largely underestimated by SOK (relative variance = 5.1), whereas OKPD produced a more realistic value (relative variance = 1.5).

Introduction

Information on soil properties can be obtained only from very small volumes, yet man frequently wants to know what the soil is like everywhere. Some form of spatial prediction is therefore needed. Basically two different models are used for spatial prediction: soil classification linked to a soil map and spatial interpolation. Both have their limitations, as discussed by Voltz & Webster (1990). Choropleth maps classify the soil and assume abrupt changes at their boundaries separating uniform classes. Interpolation techniques, such as kriging in its ordinary form, assume that all variation is gradual. However, in reality heterogeneous areas often contain both gradual and abrupt changes of soil properties, therefore in such situations it seems sensible to combine the two.

Stratification of a region based on soil map delineations, followed by within-stratum interpolation, has been used by Stein *et al.* (1988), Voltz & Webster (1990) and Van Meirvenne *et al.* (1994). Stein *et al.* (1988) calculated a variogram for each stratum, whereas Voltz & Webster (1990) computed a pooled variogram, and Van Meirvenne *et al.* (1994) standardized the pooled variogram.

Van Meirvenne (1991) and Brus *et al.* (1996) recognized that not all delineations on a soil map are equally suitable for stratification and they used their expert knowledge to select appropriate ones. Those boundaries separating classes with clear differences in their statistical properties and which represent sharp changes between them should have the most success for improving predictions. Boundaries placed where soil changes gradually are unlikely to increase the accuracy of the prediction (Brus *et al.*, 1996). A characterization of the nature of soil map delineations could facilitate their selection. Attempts to characterize delineations have been described by Burrough (1986). Later, Burrough (1989) mapped the transitions between soil mapping units based on concepts of the fuzzy set theory. However, he did not link it with spatial interpolation. Furthermore, soil delineations of crisp boundaries may be located inaccurately in the geographical space, adding uncertainty when used for stratification. Mark & Csillag (1989) described the uncertainty of class membership near a map boundary on a continuous basis. However, they did not

Correspondence: M. Van Meirvenne. E-mail: Marc.VanMeirvenne@rug.ac.be
Received 27 May 1997; revised version accepted 21 October 1997

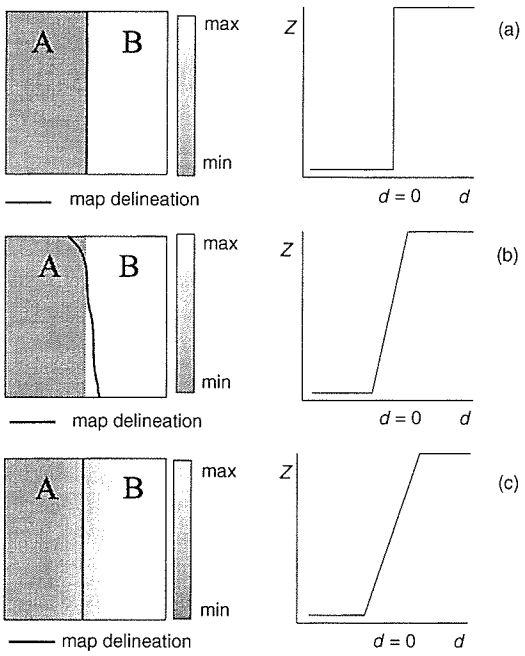

Figure 1 Choropleth soil maps consisting of two mapping classes A and B (left). The soil property Z changes abruptly in maps (a) and (b), whereas Z changes gradually in map (c). The graphs on the right present the average behaviour of Z as a function of the distance, d, to the map delineation. In map (a) the delineation coincides with a physical discontinuity ($d = 0$), in map (b) the position of the map delineation and the physical discontinuity differ substantially resulting in a gradual average change across the delineation, and in map (c) the delineation represents a gradual transition and consequently Z changes gradually across the delineation.

elaborate on this mathematically nor did they illustrate any practical applications of their modifications. Webster (1978) and Wackernagel *et al.* (1988) tried to determine the best position of soil boundaries on transects by using multivariate criteria. Our intention was not to improve the position of delineations between mapping units but to increase the usefulness of existing soil maps.

Our aims were (i) to identify the characteristics of map delineations, and (ii) to integrate the characteristics of map delineations into ordinary kriging. We applied the procedure to map the sand content of the topsoil within the province of West-Flanders, Belgium. We selected this province as a real case because of the important textural variation and because both a soil texture map (1:100 000) and a large database on soil texture were available.

Theory

Types of map delineations

A choropleth map assumes abrupt changes at its delineations, but in the real world a spatially distributed attribute Z can change abruptly or gradually across a delineation. Figure 1(a) and (c) shows that map delineations are more appropriate for delimiting abrupt discontinuities (line features) than for delimiting gradual transitions which extend over areas. For delineations representing discontinuities the positional accuracy is of particular importance. A discontinuity is accurately mapped when it coincides with the map delineation with only small divergences (Figure 1a), whereas the mapping was inaccurate when their positions differ substantially (Figure 1b). A delineation can also separate areas with a different structure of the within-unit variation.

We propose to base the identification of a map delineation on the nature of the transition, the mapping accuracy and the within-class spatial variation as given by the flow-path of Figure 2. Four types of delineations are distinguished: (i) accurate delineations of physical discontinuities, (ii) inaccurate delineations of physical discontinuities, (iii) gradual transitions separating classes with a similar structure of spatial variation, and (iv) gradual transitions separating classes with different structures of spatial variation.

Criteria for identifying the four types of map delineations

To identify the type of a map delineation we devised criteria based on point observations of the target variable. Let $\mathbf{x}_i = \{x,y\}$ be the vector of geographical coordinates of an observation i, let $d(\mathbf{x}_i)$ be the shortest distance between $\mathbf{x}_i$ and the nearest map boundary

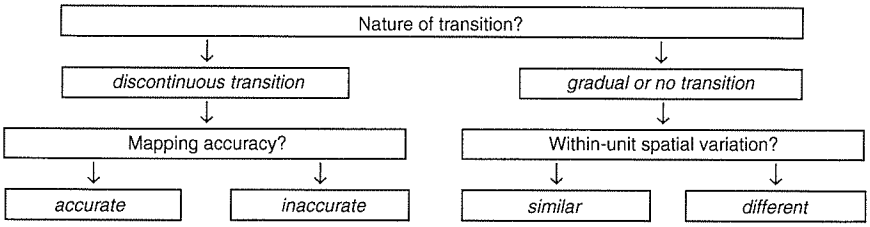

Figure 2 Flow-path for identifying the four types of map delineations based on the nature of transition, the mapping accuracy and the within-unit spatial variation.

separating two mapping classes A and B, and let $z(\mathbf{x}_i)$ be the value of soil variable Z at $\mathbf{x}_i$. Graphs of $z(\mathbf{x}_i)$ as a function of $d(\mathbf{x}_i)$ and the corresponding frequency distributions of the observations near the delineation characterize a delineation (Figure 3). As a convention, we assigned a negative sign to $d(\mathbf{x}_i)$s in class A and a positive one in class B. For all points on the delineation itself, d equals 0.

Figure 3(a) shows the situation where a physical discontinuity is accurately delineated. The observations of Z increase stepwise across the mapped boundary. Observations in class A fluctuate around a central value, z_A, those in B around a different value, z_B, and the histogram of the observations is bimodal. In this situation the map delineation coincides with the physical discontinuity of the soil variable (i.e. the discontinuity is localized at $d = 0$). Figure 3(b) shows what happens if the same physical discontinuity with the same observations is delineated inaccurately. This line on the map does not coincide with the physical discontinuity of the soil variable (i.e. the map delineation fluctuates around the physical discontinuity). The result is that some observations belonging to one class are localized inside the other. The histogram of the observations remains unchanged, of course. Because the map represents the physical discontinuity inaccurately an uncertainty zone is created (see later for definition). In Figure 3(c) and (d) Z increases gradually across the map delineation. The histograms of the observations are unimodal. In Figure 3(c) the spatial variation within the two classes A and B is similar. In Figure 3(d), however, the observations of class B vary more than those of class A: the within-class variances are different. So these gradual delineations separate two classes with similar (Figure 3c) and different (Figure 3d) spatial variations respectively.

The classification of a map delineation according to the flow-path given in Figure 2 can be based on the following criteria. First, the nature of the variation near the boundary is identified using the histogram of the observations there. If there is a strong discontinuity in Z then we might expect a large difference between the means of the two mapping classes and a dearth of observations midway between them: the histogram would be bimodal. The mapping accuracy does not affect the histogram (Figure 3a and b). Where the transition is gradual, the histogram will tend to be unimodal (Figure 3c and d). We might therefore use the histogram to identify transitions that are both abrupt and substantial, as in Figure 3(a) and (b): they will almost certainly appear bimodal. Gradual transitions will almost certainly give rise to unimodal histograms. Unfortunately, however, a unimodal histogram cannot be used as a sure diagnostic of gradual transitions because there needs to be a large difference between means in relation to the standard deviations, σ, within classes for two modes to appear. For two normal populations the difference must be greater than 2σ. To our knowledge no statistical test is available to identify the modality of a histogram. So the decision whether a histogram is unimodal or bimodal has to be based on a visual judgement of the histogram of the sample data.

Next, in the case of a discontinuous transition, the mapping accuracy is evaluated. Therefore, we fit the following function $F(z)$ to the observations near a map delineation (Figure 3a and b):

$$\begin{cases} F(z) = z_A & \text{for } d < d_A, \\ F(z) = z_A + \left(\dfrac{z_B - z_A}{d_B - d_A} \right)(d - d_A) & \text{for } d_A \leqslant d \leqslant d_B, \\ F(z) = z_B & \text{for } d > d_B, \end{cases} \quad (1)$$

with d_A, d_B, z_A and z_B the function parameters. The quantities z_A and z_B approximate the central values of the two units A and B. The distances d_A and d_B depend on the mapping accuracy and so $|d_A - d_B|$ quantifies the average width of the zone in which the physical discontinuity is located. The wider is this zone, the less accurate is the delineation and the larger the uncertainty about the position of the discontinuity. This zone is called the *uncertainty zone* U. In practice, a map delineation and a physical discontinuity will never coincide perfectly. So $|d_A - d_B|$ will never be zero. Since in practice minor divergences can be neglected, a threshold g is introduced to evaluate $|d_A - d_B|$. This threshold depends on the spatial resolution and scale of the map. If the resulting map is in raster format then g could be the diagonal of a pixel (Figure 4). If $|d_A - d_B| < g$ then the difference between the map delineation and the physical discontinuity can be neglected, and such a delineation may be regarded as accurate. If $|d_A - d_B| > g$ then the positional difference between the map delineation and the physical discontinuity cannot be neglected: it is inaccurate.

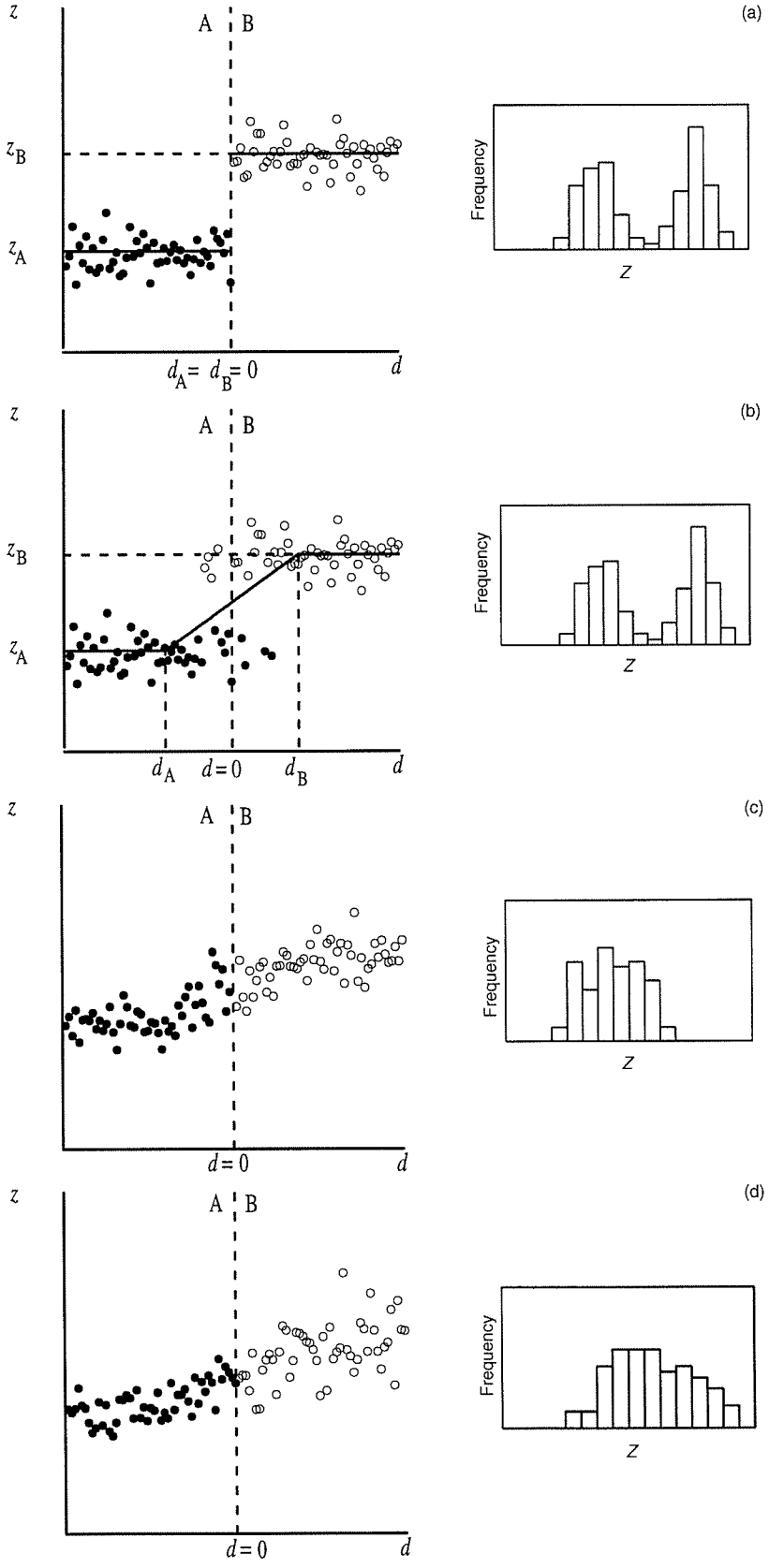
z
A
B
z_B
z_A
$d_A = d_B = 0$
d
(a)
Frequency
Z
(b)
d_A
d=0
d_B
(c)
(d)

For mapping classes separated by gradual transitions the structure of the within-class variation is compared. For this the variogram of Z can be used since it represents the structure of spatial variation of a regionalized variable, being any variable distributed in space, and soil properties can be considered to be regionalized variables. Therefore the experimental within-class variogram is calculated, and a theoretical model is fitted for each mapping class surrounded by gradual transitions. Again, as no statistical tests are available to evaluate the difference between experimental variograms this decision is subjectively based on the appearances of the variograms.

These criteria are summarized as a flow-path in Figure 5.

Ordinary kriging integrating properties of map delineations (OKPD)

Each of the four types of map delineations described above requires its particular interpolation. We used ordinary kriging as interpolation algorithm and modified it according to the type of map delineation.

Gradual transitions separating mapping units with similar structures of spatial variation. A delineation of a gradual transition between units having a similar structure of spatial variation (Figure 3c) is of little value (except to locate a threshold). Stratifying along such a line could even be a disadvantage by increasing the distance to the nearest usable observation point and thereby increasing the kriging variance (Brus *et al.*, 1996). Therefore this map delineation can be ignored and ordinary kriging (Burgess & Webster, 1980) can be preferred for interpolation across this delineation. This situation is shown in Figure 6(a). It illustrates that all neighbouring observations are used to interpolate Z at location $\mathbf{x}_0$ independently from the map delineations.

Accurately mapped physical discontinuities. The hypothesis of quasi-stationarity (Journel & Huijbregts, 1978) does not hold across accurate map delineations representing abrupt discontinuities (Figure 3a). Therefore, variogram calculations and spatial interpolation

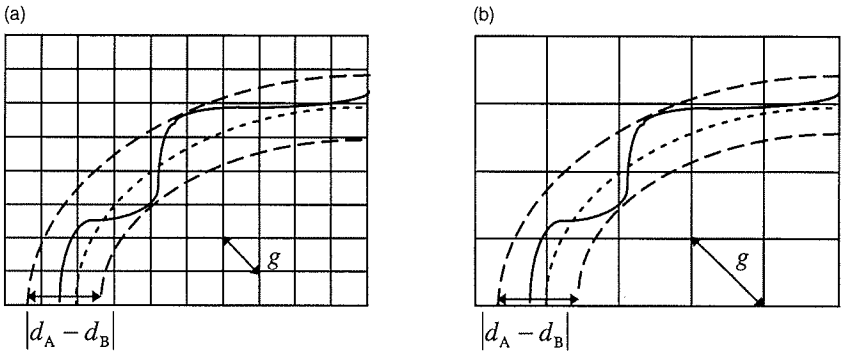

Figure 4 The threshold g depends on the resolution and scale of the final map: (a) an inaccurate delineation $|d_A - d_B| > g$; (b) an accurate delineation $|d_A - d_B| < g$. (——— physical discontinuity; - - - - - map delineation; – – – limits of the uncertainty zone.)

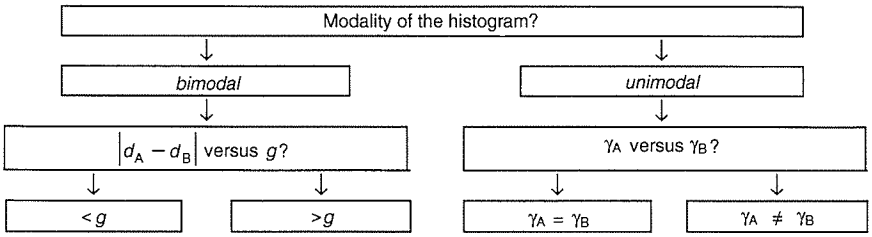

Figure 5 Criteria used to identify the four types of map delineations defined in Figure 2.

Figure 3 Four hypothetical examples in which known values of a variable, Z, belonging to two classes of soil A (●) and B (○), are plotted against their distances to a mapped boundary (left), and the histograms of these values (right). (a) The values belonging to the two distinct classes overlap neither on the Z scale nor in the geographic space, in which the boundary has been drawn accurately. (b) The values and their positions on the ground are the same as in (a), but the boundary between them has been drawn inaccurately so that it fluctuates from side to side about the true boundary. (c) There is continuous gradation in Z in the geographic space, there is overlap in Z between the two classes, and the spatial structure is the same in A and B. (d) Z varies continuously in the geographic space and there is overlap in Z between the two classes, as in (c), but class B is more variable than class A, and the boundary recognizes this difference.

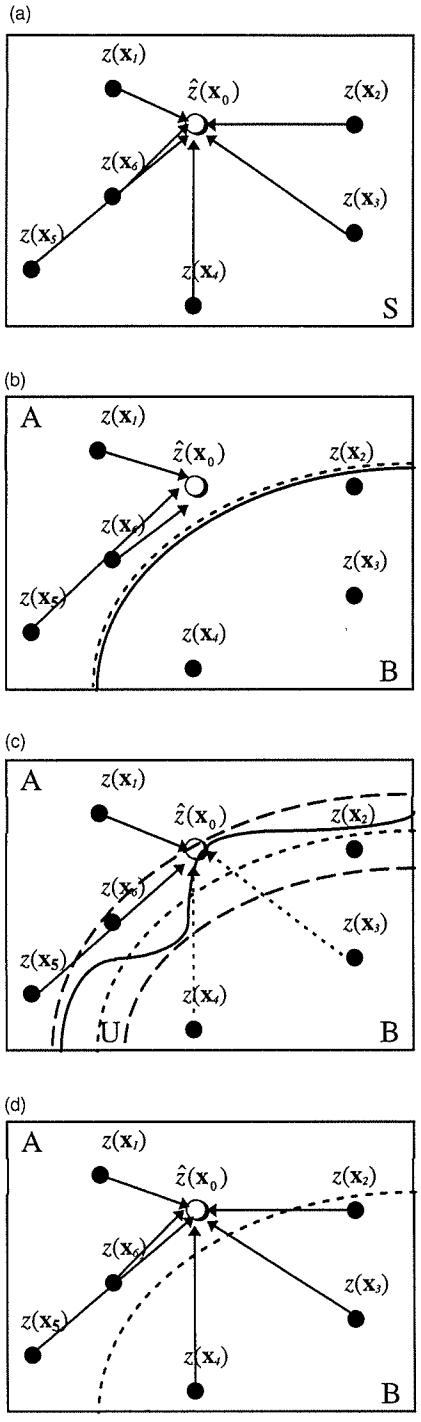

Figure 6 Illustration of the four interpolation conditions corresponding to the four types of map delineations: (a) ordinary kriging, (b) stratified ordinary kriging, (c) stratified ordinary kriging with uncertainty zone, (d) ordinary kriging with variogram stratification (arrows connect observations, $z(\mathbf{x}_i)$, used for the interpolation with the location where Z has to be interpolated, $\hat{z}(\mathbf{x}_0)$. ——— physical discontinuity; - - - - - map delineation; – – – limits of the uncertainty zone).

should be stratified. So across such delineations stratified ordinary kriging is in principle the most suitable method. Figure 6(b) illustrates this method. The area S is split into two strata A and B, with $S = A \cup B$ and $A \cap B = \varnothing$. For each stratum an experimental variogram is computed based on all observations within that stratum. For the interpolation at $\mathbf{x}_0$ only observations located in the same stratum as $\mathbf{x}_0$ are used.

Inaccurately mapped physical discontinuities. An inaccurate delineation of a discontinuity between strata creates a zone of uncertainty along the map delineation (Figure 3b). Both the discontinuity and the map delineation lie within this *uncertainty zone* U (Figure 6c). Again, the area S is split into strata A and B, with $S = A \cup B$ and $A \cap B = \varnothing$, and now with $U \subset (A \cup B)$. If the target location is outside U then there is no uncertainty to which stratum $\mathbf{x}_0$ belongs, and the following probabilities, P, are true:

$$\begin{cases} P(\mathbf{x}_0 \in A) = 1 \\ P(\mathbf{x}_0 \in B) = 0 \end{cases} \qquad \forall \mathbf{x}_0 \in A \setminus U, \tag{2}$$

and

$$\begin{cases} P(\mathbf{x}_0 \in B) = 1 \\ P(\mathbf{x}_0 \in A) = 0 \end{cases} \qquad \forall \mathbf{x}_0 \in B \setminus U. \tag{3}$$

Here $A \setminus U$ denotes the set of elements of A that do not belong to U, and $B \setminus U$ analogously for B. If $\mathbf{x}_0$ is in U then it is uncertain to which stratum it belongs, so in this situation the following probabilities apply:

$$\begin{cases} 0 < P(\mathbf{x}_0 \in A) < 1 \\ 0 < P(\mathbf{x}_0 \in B) < 1 \\ P(\mathbf{x}_0 \in A) + P(\mathbf{x}_0 \in B) = 1 \end{cases} \qquad \forall \mathbf{x}_0 \in U. \tag{4}$$

We can define the probabilities as functions of the distance to the map boundary $d(\mathbf{x}_0)$. Let us assume symmetry, so that the uncertainty to which stratum $\mathbf{x}_0$ belongs is maximal, i.e. $P(\mathbf{x}_0 \in B) = P(\mathbf{x}_0 \in A) = 0.5$, at the centre of U, i.e. at $d = (d_A - d_B/2)$. Let us also assume that these probabilities change linearly towards the borders of U, so

$$\begin{cases} P(\mathbf{x}_0 \in A) = \dfrac{d(\mathbf{x}_0) - d_B}{d_A - d_B} \\ P(\mathbf{x}_0 \in B) = 1 - \dfrac{d(\mathbf{x}_0) - d_B}{d_A - d_B} \end{cases} \qquad \text{for } d_A \leqslant d(\mathbf{x}_0) \leqslant d_B. \tag{5}$$

For every stratum a within-stratum sample variogram of Z is calculated using observations $z(\mathbf{x}_i)$ belonging unequivocally to that stratum:

$$\gamma_A(\mathbf{h}) = \frac{1}{2N_A(\mathbf{h})} \sum_{i=1}^{N_A(\mathbf{h})} \{z(\mathbf{x}_i) - z(\mathbf{x}_i + \mathbf{h})\}^2 \qquad \forall \mathbf{x}_i, \mathbf{x}_i + \mathbf{h} \in A \setminus U, \tag{6}$$

and

$$\gamma_B(\mathbf{h}) = \frac{1}{2N_B(\mathbf{h})} \sum_{i=1}^{N_B(\mathbf{h})} \{z(\mathbf{x}_i) - z(\mathbf{x}_i + \mathbf{h})\}^2 \qquad \forall \mathbf{x}_i, \mathbf{x}_i + \mathbf{h} \in B \setminus U. \tag{7}$$

In these equations $N_A(\mathbf{h})$ and $N_B(\mathbf{h})$ are the numbers of pairs involved in the calculation of the semivariances at lag $\mathbf{h}$, $\gamma_A(\mathbf{h})$ and $\gamma_B(\mathbf{h})$. Observations within U are excluded because we do not know to which stratum they belong. Models are fitted to the experimental variograms, and two interpolation estimates are produced by ordinary kriging for each point $\mathbf{x}_0$. One estimate, $\hat{z}_A(\mathbf{x}_0)$, is based on variogram $\gamma_A(\mathbf{h})$ and the observations in $A \setminus U$. A second estimate, $\hat{z}_B(\mathbf{x}_0)$, is based on variogram $\gamma_B(\mathbf{h})$ and the observations in $B \setminus U$. Observations within U are not used. So:

$$\hat{z}_A(\mathbf{x}_0) = \sum_{i=1}^{n} \lambda_{A,i} z(\mathbf{x}_i), \qquad \mathbf{x}_i \in (A \setminus U), \forall \mathbf{x}_0 \in S, \tag{8}$$

and

$$\hat{z}_B(\mathbf{x}_0) = \sum_{i=1}^{n} \lambda_{B,i} z(\mathbf{x}_i), \qquad \mathbf{x}_i \in (B \setminus U), \forall \mathbf{x}_0 \in S, \tag{9}$$

with $\lambda_{A,i}$ and $\lambda_{B,i}$ the weights attached to the n observations involved in the interpolation. The weights are found by solving the kriging systems:

$$\sum_{i=1}^{n} \lambda_{A,i} \gamma(\mathbf{x}_j, \mathbf{x}_i) + \varphi_A = \gamma_A(\mathbf{x}_j, \mathbf{x}_0), \qquad j = 1, \ldots, n \qquad \mathbf{x}_i, \mathbf{x}_j \in (A \setminus U), \forall \mathbf{x}_0 \in S \tag{10}$$

$$\sum_{i=1}^{n} \lambda_{A,i} = 1 \tag{11}$$

and

$$\sum_{i=1}^{n} \lambda_{B,i}\,\gamma(\mathbf{x}_j, \mathbf{x}_i) + \varphi_B = \gamma_B(\mathbf{x}_j, \mathbf{x}_0), \qquad j = 1, \ldots, n \qquad \mathbf{x}_i, \mathbf{x}_j \in (B \setminus U), \forall \mathbf{x}_0 \in S \tag{12}$$

$$\sum_{i=1}^{n} \lambda_{B,i} = 1. \tag{13}$$

The estimation variances are defined by

$$\hat{\sigma}^2_A(\mathbf{x}_0) = \varphi_A + \sum_{i=1}^{n} \lambda_{A,i}\gamma_A(\mathbf{x}_i, \mathbf{x}_0), \qquad \mathbf{x}_i \in (A \setminus U), \forall \mathbf{x}_0 \in S, \tag{14}$$

and

$$\hat{\sigma}^2_B(\mathbf{x}_0) = \varphi_B + \sum_{i=1}^{n} \lambda_{B,i}\gamma_B(\mathbf{x}_i, \mathbf{x}_0), \qquad \mathbf{x}_i \in (B \setminus U), \forall \mathbf{x}_0 \in S, \tag{15}$$

where φ_A and φ_B are the Lagrange multipliers.

Combining the two estimates gives an unconditional estimate of Z and its ordinary kriging variance (see the Appendix for the derivation):

$$\hat{z}(\mathbf{x}_0) = P(\mathbf{x}_0 \in A)\hat{z}_A(\mathbf{x}_0) + P(\mathbf{x}_0 \in B)\hat{z}_B(\mathbf{x}_0), \tag{16}$$

and

$$\hat{\sigma}^2(\mathbf{x}_0) = P(\mathbf{x}_0 \in A)^2\hat{\sigma}^2_A(\mathbf{x}_0) + P(\mathbf{x}_0 \in B)^2\hat{\sigma}^2_B(\mathbf{x}_0) + P(\mathbf{x}_0 \in A)P(\mathbf{x}_0 \in B)[\{\hat{z}_A(\mathbf{x}_0) - \hat{z}_B(\mathbf{x}_0)]\}^2 + c_A + c_B], \tag{17}$$

in which c_A and c_B are the sills of the variograms of strata A and B. If $\mathbf{x}_0$ is outside U then this reduces to the estimates $z_A(\mathbf{x}_0)$ and $\hat{\sigma}^2_A(\mathbf{x}_0)$ for $\mathbf{x}_0 \in A \setminus U$ or $\hat{z}_B(\mathbf{x}_0)$ and $\hat{\sigma}^2_B(\mathbf{x}_0)$ for $\mathbf{x}_0 \in B \setminus U$.

Gradual transitions separating mapping units with different structures of spatial variation. In the case that the delineation represents a gradual transition separating two strata with different structures of spatial variation (Figure 3d), separate within-stratum variograms have to be calculated:

$$\gamma_A(\mathbf{h}) = \frac{1}{2N_A(\mathbf{h})}\sum_{i=1}^{N_A(\mathbf{h})} \{z(\mathbf{x}_i) - z(\mathbf{x}_i + \mathbf{h})\}^2 \qquad \forall \mathbf{x}_i, \mathbf{x}_i + \mathbf{h} \in A, \tag{18}$$

and

$$\gamma_B(\mathbf{h}) = \frac{1}{2N_B(\mathbf{h})}\sum_{i=1}^{N_B(\mathbf{h})} \{z(\mathbf{x}_i) - z(\mathbf{x}_i + \mathbf{h})\}^2 \qquad \forall \mathbf{x}_i, \mathbf{x}_i + \mathbf{h} \in B. \tag{19}$$

Ordinary kriging is performed across the gradual transitions with the kriging weights determined only by the variogram of the stratum to which $\mathbf{x}_0$ belongs (Figure 6d):

$$\hat{z}(\mathbf{x}_0) = \sum_{i=1}^{n} \lambda_{A,i} z(\mathbf{x}_i), \qquad \mathbf{x}_i \in S, \forall \mathbf{x}_0 \in A, \tag{20}$$

and

$$\hat{z}(\mathbf{x}_0) = \sum_{i=1}^{n} \lambda_{B,i} z(\mathbf{x}_i), \qquad \mathbf{x}_i \in S, \forall \mathbf{x}_0 \in B. \tag{21}$$

The weights are found by solving the kriging systems:

$$\sum_{i=1}^{n} \lambda_{A,i}\gamma(\mathbf{x}_j, \mathbf{x}_i) + \varphi_A = \gamma_A(\mathbf{x}_j, \mathbf{x}_0), j = 1, \ldots, n \qquad \mathbf{x}_i, \mathbf{x}_j \in S, \forall \mathbf{x}_0 \in A \tag{22}$$

$$\sum_{i=1}^{n} \lambda_{A,i} = 1 \tag{23}$$

and

$$\sum_{i=1}^{n} \lambda_{B,i}\gamma(\mathbf{x}_j, \mathbf{x}_i) + \varphi_B = \gamma_B(\mathbf{x}_j, \mathbf{x}_0), j = 1, \ldots, n \qquad \mathbf{x}_i, \mathbf{x}_j \in S, \forall \mathbf{x}_0 \in B \tag{24}$$

$$\sum_{i=1}^{n} \lambda_{B,i} = 1. \tag{25}$$

The estimation variances are given by:

$$\hat{\sigma}^2(\mathbf{x}_0) = \varphi_A + \sum_{i=1}^{n} \lambda_{A,i}\gamma_A(\mathbf{x}_i, \mathbf{x}_0), \qquad \mathbf{x}_i \in S, \forall \mathbf{x}_0 \in A, \tag{26}$$

and

$$\hat{\sigma}^2(\mathbf{x}_0) = \varphi_B + \sum_{i=1}^{n} \lambda_{B,i}\gamma_B(\mathbf{x}_i, \mathbf{x}_0), \qquad \mathbf{x}_i \in S, \forall \mathbf{x}_0 \in B. \tag{27}$$

Thus in this case, the delineation is used to stratify the variogram but not the observations involved in the interpolation.

Case study: topsoil sand content of West-Flanders

Study region and data

The inventory of the sand content of the topsoil of the province of West-Flanders, covering 3144 km^2 in Belgium, provided data to illustrate the approach discussed above for two reasons. First, the soil derives from varied geology and parent material, and so there is much textural variety. Secondly, a 1:100 000 regional map of soil texture is available (De Leenheer & Appelmans, 1975), and there are data of topsoil sand for 2608 sites. Moreover, knowledge of the geological history and soil genesis allows us to interpret the results.

The database was built by correcting and completing the digital database of the National Soil Survey (De Leenheer *et al.*, 1968; Van Orshoven *et al.*, 1988) and enlarging it with data from additional studies by De Leenheer & Van Ruymbeke (1960), De Smet *et al.* (1996) and ourselves. Samples were taken both from soil horizons and at fixed depths, depending on the survey, and so we recalculated sand content to a standard depth of 0–30 cm. An independent validation data set was formed by randomly selecting 475 data (18%) of the available 2608 observations. The remaining 2133 observations were used for the following analysis.

The soil texture map was generalized into five classes (Figure 7). The variation of the topsoil sand content within these was characterized using the 2133 data of topsoil sand. Table 1 summarizes the statistics. There are important differences both in the mean sand content and in the within-unit variances. The most heterogeneous mapping unit is the Polders, the most homogeneous are the Silty Sand and Sand units. The sample density was fairly uniform, ranging from 0.6 to 1 sample per km^2. The intraclass correlation coefficient (Webster & Beckett, 1968) of the generalized texture map was 0.59, so this map can be considered to be successful in delineating differences in topsoil sand content to some extent, since it accounts for about 59% of the spatial variation. The mapping units can be combined into three pedogenetic groups representing the major differences in parent material and geological genesis encountered in the province, as follows.

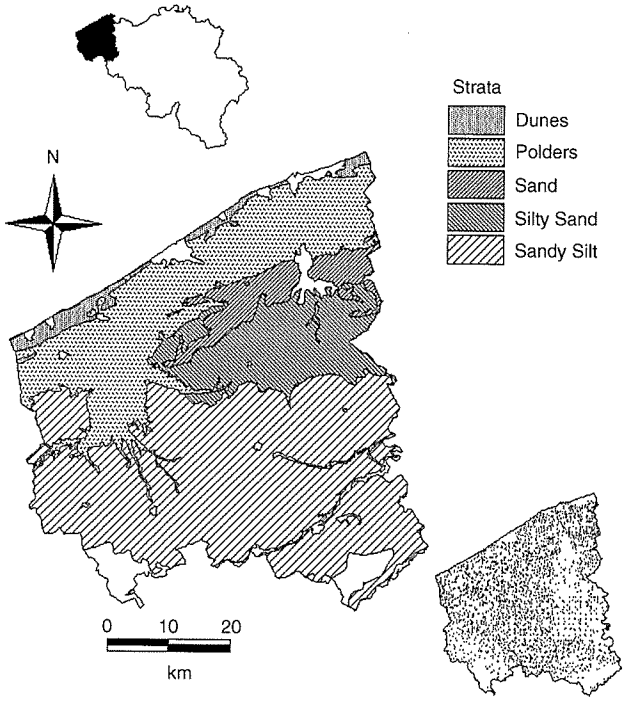

Figure 7 Generalized soil texture map of West-Flanders (scale of publication is 1:100 000), with location of West-Flanders inside Belgium (top left map) and indication of the sampling locations (bottom right map).

Table 1 Statistics of the 2133 texture analyses grouped according to the units of the soil texture map ($\bar{z}$, mean value; s^2, variance)

Mapping unit	Number of data	$\bar{z}$ /%	s^2 /%^{2}	5th percentile /%	95th percentile /%	Area /km^2	Sample density /km^{-2}
Dunes	61	90	267	53	99	84	0.73
Polders	774	32	471	5	75	783	0.99
Sand	125	89	153	64	96	174	0.76
Silty Sand	234	74	104	53	87	400	0.58
Sandy Silt	939	53	266	23	78	1512	0.62

1 *Dunes*. This unit represents wind-blown and recently deposited sandy material (average sand content 90%; Table 1). However, inside this mapping unit texture varies from sand to clay. Field verification confirmed that the observation points with clayey texture represent small parts of the adjacent polder area interfingering into this unit, but these do not appear on the map. Evidently the map delineation does not accurately follow all details of the physical discontinuity.
2 *Polders*. The region behind the Dunes was flooded during historical times and transformed into a polder by man. A highly variable texture is typical for this polder and is reflected in the large variance of topsoil sand content (471%^{2}) and the difference between the 5th and 95th percentiles (Table 1).
3 *Wind-blown sediments*. The largest part of the province is covered by Pleistocene wind-blown sediments. Generally, from north to south the following sequence of mapping units is found: Sand, Silty Sand and Sandy Silt (Figure 7). However, locally this general behaviour is disturbed by differences in topography. Within these units texture is less variable (Table 1).

Characterization of the map delineations

The soil texture map contains six map delineations: Dunes–Polders, Polders–Sand, Polders–Silty Sand, Polders–Sandy Silt, Sand–Silty Sand, and Silty Sand–Sandy Silt. First, the frequency distributions of the data near these delineations, i.e. for $d(\mathbf{x}_i) \leqslant 2000$ m, were calculated (Figure 8). The histograms of the Dunes–Polders (Figure 8a), Sand–Polders (Figure 8b), Silty Sand–Polders (Figure 8c) and Sandy Silt–Polders (Figure 8d) delineations indicate multimodal distributions whereas histograms of the Sand–Silty Sand (Figure 8e) and Silty Sand–Sandy Silt (Figure 8f) delineations tend to unimodal distributions. These findings confirm our expectation that discontinuities occur at delineations between units of different geological genesis and gradual transitions are encountered between units with a similar geological genesis.

Next, the accuracy of delineations of a discontinuity has to be evaluated. Figure 9 shows the sand content as a function of the shortest distance to the nearest map delineation. For delineations of discontinuities (Figure 9a–d), Equation (1) was fitted to the observations, and the values of $|d_A - d_B|$ are given in Table 2. The final map is intended to have a spatial resolution of 200 m × 200 m raster cells, so the threshold g was taken to be 300 m. Since all delineations of a physical discontinuity had a $|d_A - d_B|$ larger than 300 m, they were all identified as inaccurate (Table 2).

Two delineations, Sand–Silty Sand and Silty Sand–Sandy Silt, were identified as delimiting gradual transitions due to the unimodal appearance of the frequency distribution. So following the flow-path of Figure 5, the within-unit structure of spatial variation has to be characterized. The experimental variogram of the units Sand, Silty Sand and Sandy Silt was calculated excluding data within the uncertainty zones along the four inaccurate delineations Dunes–Polders, Polders–Sand, Polders–Silty Sand, Polders–Sandy Silt. Two isotropic models were fitted to the experimental variogram using a least-squares criterion. They were as follows:

The spherical model:

$$\begin{cases} \gamma(h) = c_0 + c \left\{ \dfrac{3h}{2a} - \dfrac{1}{2}\left(\dfrac{h}{a}\right)^3 \right\} & \text{for } 0 < h \leqslant a \\ \gamma(h) = c_0 + c & \text{for } h < a \\ \gamma(0) = 0, \end{cases} \tag{28}$$

with $\gamma(h)$ the semivariance at lag distance h, c_0 the nugget variance, c the sill of the correlated variance and a the range; and

The linear model:

$$\begin{cases} \gamma(0) = 0 \\ \gamma(h) = c_0 + bh \qquad \text{for } h > 0, \end{cases} \tag{29}$$

where b is the slope.

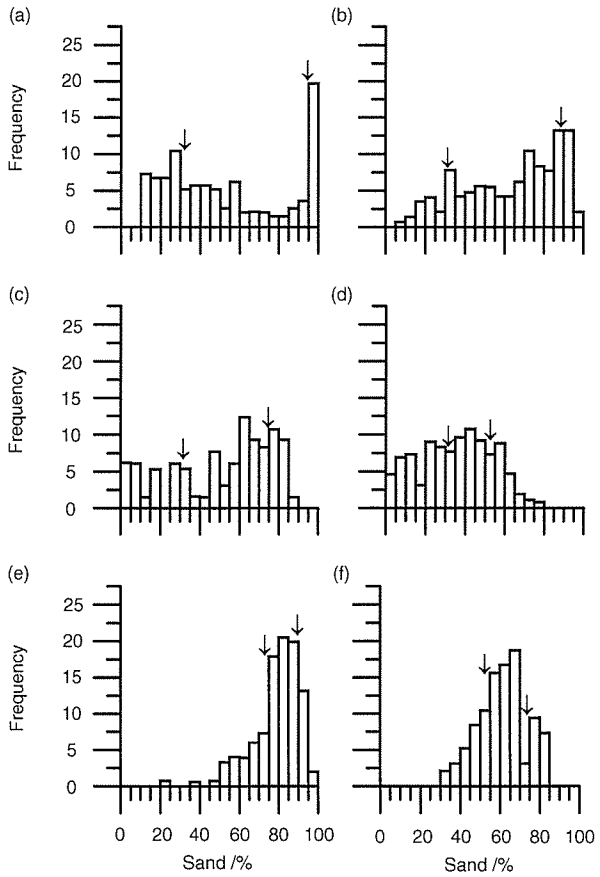

Figure 8 Frequency distributions of data near delineations, i.e. for $d(\mathbf{x}_i) < 2000$ m: (a) Dunes–Polders; (b) Sand–Polders; (c) Silty Sand–Polders; (d) Sandy Silt–Polders; (e) Sand–Silty Sand; (f) Silty Sand–Sandy Silt. Arrows indicate the average sand contents of the two mapping classes involved (Table 1).

Table 3 gives the Akaike Information Criterion (AIC) (Webster & McBratney, 1989) for the selection of the best fitting model and the model parameters of the retained model. Figure 10 presents the sample variograms and the fitted models. Based on a visual judgement of Figure 10(d)–(f), we concluded that the variograms calculated without the observations inside the uncertainty zones of units Sand, Silty Sand and Sandy Silt were different (Table 2).

So four delineations were identified as inaccurate delineations of discontinuities. The remaining two were identified as delineations of gradual transitions between mapping units with different structures of spatial variation. So only the situations illustrated in Figure 3(b) and (d) were found in our case study. According to the flow-path of Figure 5, the first four map delineations require stratified ordinary kriging with an uncertainty zone, and the last two delineations call for ordinary kriging with variogram stratification.

Validation

We compared ordinary kriging integrating properties of map delineations (OKPD), the method developed in this paper, with stratified ordinary kriging (SOK). The latter treats all retained map delineations in the same way, i.e. as sharp discontinuities, whereas in OKPD the properties of each map delineation are identified and subsequently integrated in the kriging interpolation as described above. Ordinary kriging (OK) (without stratification) was added as a reference.

To compare these three approaches the global variogram using all observations was calculated for OK (Table 4 and Figure 10a), and within-unit variograms were calculated using (i) all observations within each stratum for SOK (Table 4 and Figure 10b–f) and (ii) only those observations outside the uncertainty zones of the inaccurately mapped delineations for OKPD (Table 3 and Figure 10b–f). For the Dunes the latter resulted in a dramatic decrease of the semivariance, as most clayey samples lie within the uncertainty zone (Figure 10b).

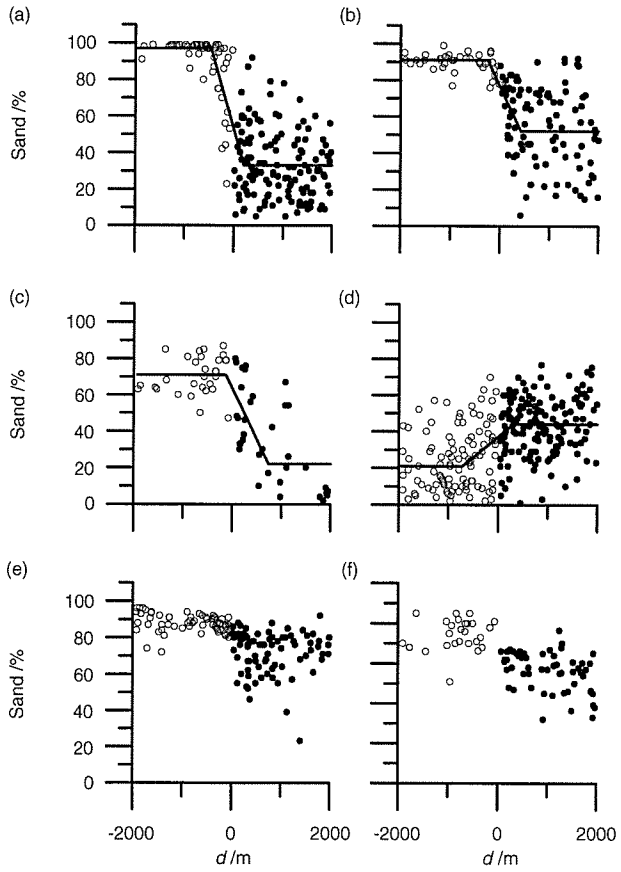

Figure 9 Plots of z as functions of d: (a) Dunes (○)–Polders (●); (b) Sand (○)–Polders (●); (c) Silty Sand (○)–Polders (●); (d) Sandy Silt (○)–Polders (●); (e) Sand (○)–Silty Sand (●); (f) Silty Sand (○)–Sandy Silt (●).

Table 2 Characterization of map delineations

		Mapping accuracy		
Map delineations	Physical nature	$\lvert d_A - d_B \rvert$ /m		Spatial variation
Dunes–Polders	discontinuity	663	inaccurate	–
Sand–Polders	discontinuity	673	inaccurate	–
Silty Sand–Polders	discontinuity	871	inaccurate	–
Sandy Silt–Polders	discontinuity	1027	inaccurate	–
Sand–Silty Sand	gradual transition	–	–	different
Silty Sand–Sandy Silt	gradual transition	–	–	different

The performance of OK, SOK and OKPD was evaluated, using the independent validation set of 475 data, in terms of three indices: the mean prediction error (*MPE*), the mean square prediction error (*MSPE*) and the relative variance (*RV*), defined as:

$$MPE = \frac{1}{n} \sum_{i=1}^{n} \{z(\mathbf{x}_i) - \hat{z}(\mathbf{x}_i)\}, \tag{30}$$

$$MSPE = \frac{1}{n} \sum_{i=1}^{n} \{z(\mathbf{x}_i) - \hat{z}(\mathbf{x}_i)\}^2, \tag{31}$$

and

Table 3 Akaike Information Criterion (AIC) used to select the best theoretical variogram model and parameters of the retained model. Observations in the uncertainty zones of inaccurate delineations were excluded from variogram calculations

	AIC						
	Linear	Spherical	Retained model	c_0 /%^{2}	c /%^{2}	a /m	b /%^{2} m^{-1}
Dunes	41	47	Linear	7	–	–	0.00215
Polders	196	182	Spherical	182	403	13 620	–
Sand	21	9	Spherical	10	27	2 208	–
Silty Sand	157	147	Spherical	49	96	4 076	–
Sandy Silt	160	107	Spherical	95	208	10 901	–

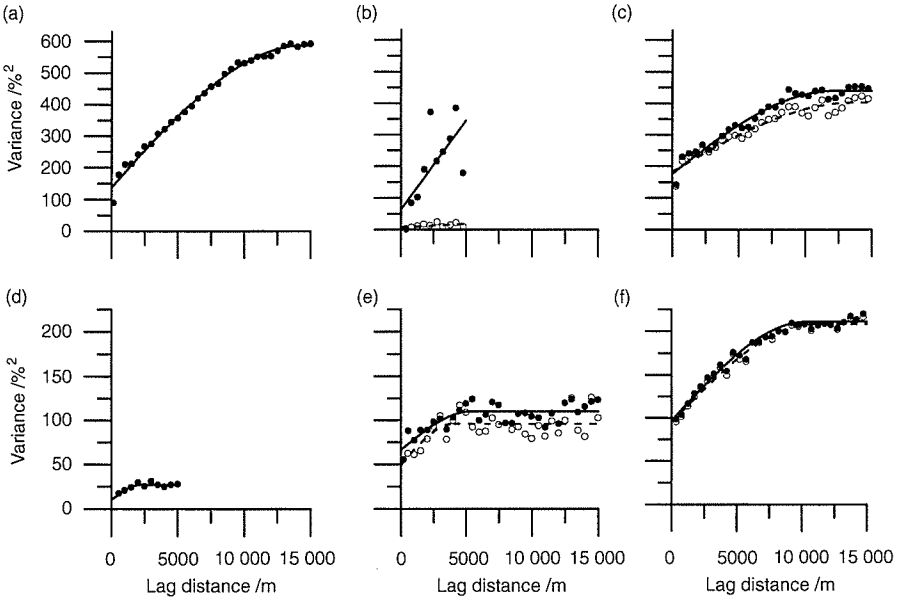

Figure 10 Experimental (points) and theoretical (curves) variograms of (a) the entire study area (without stratification) and of each stratum separately: (b) Dunes; (c) Polders; (d) Sand; (e) Silty Sand; (f) Sandy Silt (—●—)using all observations within the stratum and - - -○- - - using observations within the stratum but outside the uncertainty zone).

$$RV = \frac{1}{n} \sum_{i=1}^{n} \frac{\{z\mathbf{x}_i) - \hat{z}(\mathbf{x}_i)\}^2}{\hat{\sigma}^2(\mathbf{x}_i)}. \tag{32}$$

In these equations $z(\mathbf{x}_i)$ is the observed value of Z at validation point $\mathbf{x}_i$, $\hat{z}(\mathbf{x}_i)$ is the predicted value at the same validation point, $\hat{\sigma}^2(\mathbf{x}_i)$ is the kriging variance at validation point $\mathbf{x}_i$, and n is the number of validation points. The prediction is unbiased when *MPE* equals 0. The *MSPE* is a measure of the average precision of the prediction, and so it should be as small as possible. A $RV > 1$ indicates that the kriging variance underestimates the true prediction variance; the reverse holds if $RV < 1$. Therefore, *RV* should be close to 1.

Table 5 shows the result of the validation of OK, SOK and OKPD. First, let us consider the indices computed on all 475 validation points. Stratified kriging (SOK) scores better than OK as indicated by *MPE* and *MSPE*, although the *RV* was slightly larger. So we concluded that stratification makes sense. The validation indices of SOK and OKPD were almost equal. The *MPE*s are close to zero, and the *MSPE* of OKPD (171%^{2}) was somewhat smaller than the *MSPE* of SOK (178%^{2}). However, we must realize that (i) the soil texture map is successful in stratifying the area (an intraclass correlation coefficient of 0.51), leaving a limited margin to demonstrate improvements between two similar interpolation procedures both relying on this map, and (ii) the major differences between SOK and OKPD are situated near the map delineations and these areas represent only a minor part of

Table 4 Akaike Information Criterion (AIC) used to select the best theoretical variogram model and parameters of the retained model. All observations were used for variogram calculations

	AIC						
	Linear	Spherical	Retained model	c_0 /%^{2}	c /%^{2}	a /m	b /%^{2} m^{-1}
Global variogram	317	262	Spherical	137	450	14 353	–
Dunes	95	105	Linear	63	–	–	0.0562
Polders	208	177	Spherical	176	440	12 117	–
Sand	21	9	Spherical	10	27	2 208	–
Silty Sand	151	136	Spherical	66	110	5 399	–
Sandy Silt	159	107	Spherical	97	211	10 429	–

Table 5 Mean prediction error (*MPE*), mean square prediction error (*MSPE*) and relative variance (*RV*) of topsoil sand for OK, SOK and OKPD

	All validation points (n = 475)			Validation points in uncertainty zones (n = 19)		Validation points nearby gradual transitions (n = 36)		Remaining validation points (n = 420)	
	OK	SOK	OKPD	SOK	OKPD	SOK	OKPD	SOK	OKPD
MPE /%	–0.71	–0.03	–0.27	3.18	0.31	–1.39	–1.36	–0.11	–0.23
MSPE /%^{2}	191	178	171	824	530	60	61	159	164
RV	1.01	1.20	1.22	5.06	1.48	1.04	1.14	1.04	1.25

the total area (about 5%). Therefore, we split the validation data set into three parts: (i) points inside the uncertainty zones, (ii) points near delineations, i.e. $d(\mathbf{x}_i) < 500$, representing gradual transitions, and (iii) the remaining points where we can expect that SOK and OKPD will perform similarly.

The indices (Table 5) computed on the points near gradual transitions and those computed on the remaining were almost equal for SOK and OKPD. In this case study, the modifications of the ordinary kriging algorithm at delineations of gradual transitions separating units with a different structure of spatial variation (ordinary kriging and ordinary kriging with variogram stratification) did not result in a better prediction. However, inside the uncertainty zones OKPD performed much better than SOK both for the kriging estimate and for its associated kriging variance. For OKPD the *MPE* was closer to zero, the *MSPE* decreased substantially, and the *RV* was closer to 1. The indices indicated also that both SOK and OKPD performed better outside the uncertainty zones than in it, so these clearly are zones where it is difficult to predict the sand content.

Interpolation

Maps of the prediction estimate and variance of topsoil sand were produced using both SOK and OKPD using all data. Punctual kriging was used with a resolution of 200 m × 200 m. Figure 11 shows the result of a part of the province, including parts of the mapping units Dunes, Polders, Sand and Silty Sand (Figure 7). With OKPD uncertainty zones were defined along the delineations Dunes–Polders, Polders–Sand and Polders–Silty Sand. On the SOK map (Figure 11b) the sand content changes discontinuously at all delineations, whereas on the OKPD map (Figure 11a) sand content changes gradually at the inaccurately mapped delineation and at delineations of gradual transitions. More obvious differences exist between the kriging variances (Figure 11c and d): for OKPD the kriging variances were considerably larger in the uncertainty zones and considerably smaller inside the mapping units (particularly for the mapping unit Dunes) because of the large difference in variogram models. Kriging variances were larger along inaccurately mapped delineations associated with the uncertainty resulting from the inaccurate placing of this boundary. Despite the inaccurate positions of delineations, the information they represent was included in the prediction, but the price paid for this uncertain information is an inflation of the kriging variance near these delineations.

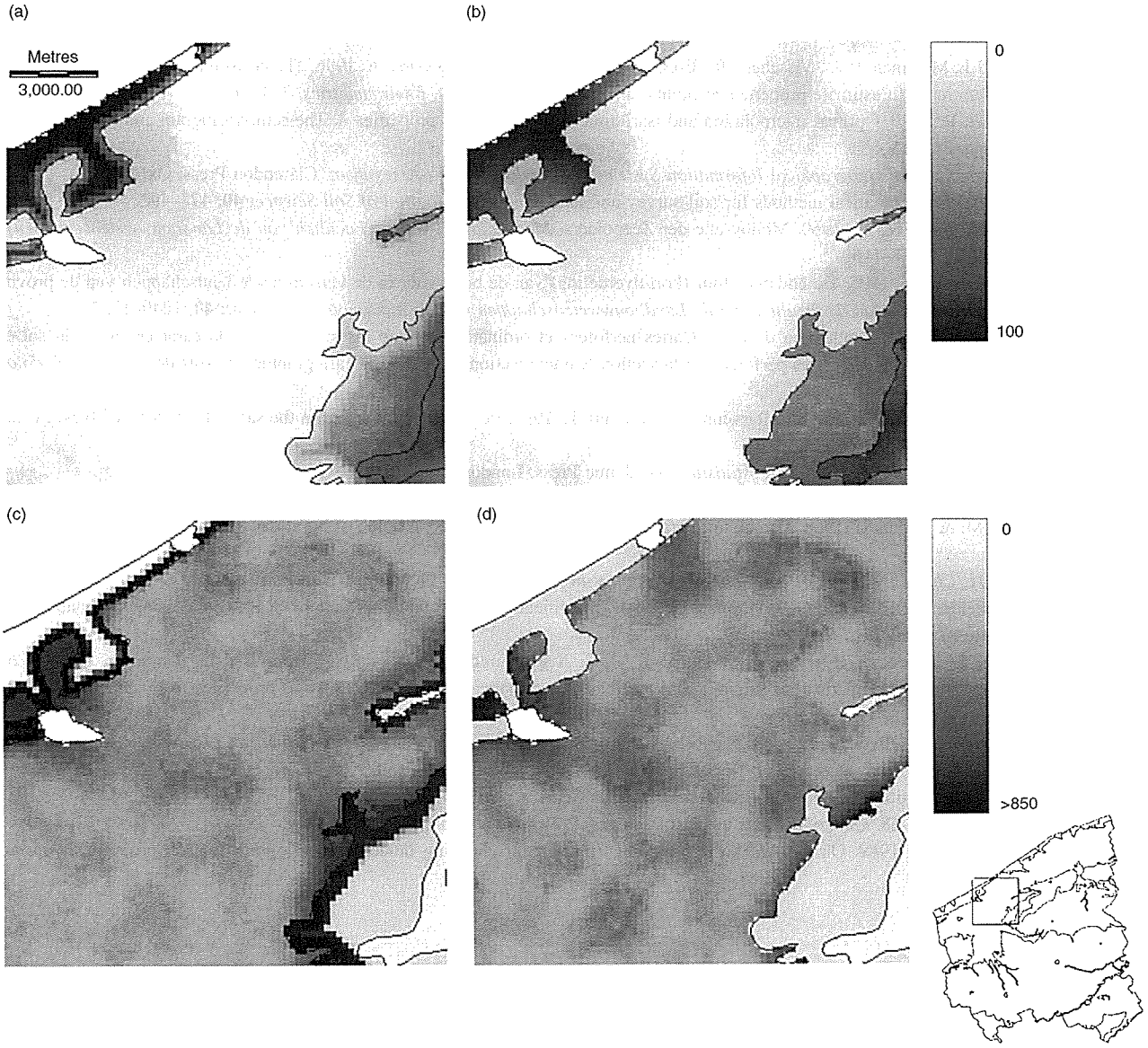

Figure 11 Kriging estimates (%) (a and b) and kriging variances (%^{2}) (c and d) of topsoil sand for OKPD (a and c) and SOK (b and d) for a part of the province.

Conclusions

The test case showed that the proposed methodology (OKPD) can be used if one has sufficiently dense data to characterize the map delineations and to calculate the within-unit variograms. Validation indicated that the benefits of the proposed kriging modifications were most apparent in the uncertainty zones. Therefore we feel that the procedure could be valuable in situations where the inventory is obtained by interpolating point data using a stratification based on a soil map which contains inaccurate delineations of physical discontinuities.

Acknowledgements

We thank Dr G.B.M. Heuvelink and Dr R. Webster for their valuable comments and Ir J. Biesemans for helping us to improve our computing.

References

Brus, D.J., De Gruijter, J.J., Marsman, B.A., Visschers, R., Bregt, A.K., Bouma, J. & Breeuwsma, A. 1996. The performance of spatial interpolation methods and choropleth maps to estimate properties at points: a soil survey case study. *Environmetrics,* **7**, 1–16.

Burgess, T.M. & Webster, R. 1980. Optimal interpolation and isarithmic mapping of soil properties. I. The semi-variogram and punctual kriging. *Journal of Soil Science*, **31**, 315–331.

Burrough, P.A. 1986. *Principles of Geographical Information Systems for Land Resources Assessment.* Clarendon Press, Oxford.

Burrough, P.A. 1989. Fuzzy mathematical methods for soil survey and land evaluation. *Journal of Soil Science*, **40**, 477–492.

De Leenheer, L. & Van Ruymbeke, M. 1960. Monografie der Zeepolders. *Mededelingen van de Faculteit van de Landbouwwetenschappen van de Rijksuniverstiteit Gent*, **25**, 1–416.

De Leenheer, L. & Appelmans, F. 1975. De bodemtextuur (korrelverdeling) van de bouwvoor in de verschillende landschappen van de provincie West-Vlaanderen. *Mededelingen van de faculteit van de Landbouwwetenschappen van de Rijksuniverstiteit Gent*, **40**, 1249–1332.

De Leenheer, L., Appelmans, F. & Vandamme, J. 1968. Cartes perforées et ordinateur comme instruments pour la caractérisation du sol et la pédologie régionale – Le système des cartes perforées de la section 'caractérisation du sol' de la cartographie des sols de Belgique. *Pedologie*, **18**, 208–227.

De Smet, J., Hofman, G., Vanderdeelen, J., Van Meirvenne, M. & Baert, L. 1996. Phosphate enrichment in the sandy loam soils of West-Flanders, Belgium. *Fertilizer Research*, **43**, 209–215.

Journel, A.G. & Huijbregts, C.J. 1978. *Mining Geostatistics.* Academic Press, London.

Mark, D.M. & Csillag, F. 1989. The nature of boundaries on 'Area-Class' maps. *Cartographica*, **26**, 65–78.

Stein, A., Hoogerwerf, M. & Bouma, J. 1988. Use of soil-map delineations to improve (co-)kriging of point data on moisture deficits. *Geoderma,* **43**, 163–177.

Van Meirvenne, M. 1991. *Characterization of Soil Spatial Variation using Geostatistics.* PhD thesis, University of Gent.

Van Meirvenne, M., Scheldeman, K., Baert, G. & Hofman, G. 1994. Quantification of soil textural fractions of Bas-Zaire using soil map polygons and/or point observations. *Geoderma*, **62**, 69–82.

Van Orshoven, J., Maes, J., Vereecken, H., Feyen, J. & Dudal, R. 1988. A structured database of Belgian profile data. *Pedologie*, **38**, 191–206.

Voltz, M. & Webster, R. 1990. A comparison of kriging, cubic splines and classification for predicting soil properties from sample information. *Journal of Soil Science*, **41**, 473–490.

Wackernagel, H., Webster, R. & Oliver, M.A. 1988. A geostatistical method for segmenting multivariate sequences of soil data. In: *Classification and Related Methods of Data Analysis* (ed. H.H. Bock), pp. 641–650. Elsevier-North Holland, Amsterdam.

Webster, R. 1978. Optimally partitioning soil transects. *Journal of Soil Science*, **29**, 388–402.

Webster, R. & Beckett, P.H.T. 1968. Quality and usefulness of soil maps. *Nature, London*, **219**, 680–682.

Webster, R. & McBratney, A.B. 1989. On the Akaike Information Criterion for choosing models for variograms of soil properties. *Journal of Soil Science*, **40**, 493–496.

Appendix

In stratum K (K = A,B) kriging is based on the model:

$$Z_K(\mathbf{x}) = \mu_K + \delta_K(\mathbf{x}) \qquad \mathbf{x} \in K, \tag{A1}$$

where μ_K is the mean of the random variable Z in stratum K, $\delta_K(\mathbf{x})$ is a random variable with variogram of stratum K, and $\mathbf{x}$ is a position vector.

Kriging predictor

Within the uncertainty zone every point $\mathbf{x}_0$ belongs to either A or B but for no point is it known to which stratum it belongs. The conditional predictions generated by stratified ordinary kriging can be combined into an unconditional expected value at $\mathbf{x}_0$ given by:

$$\mathrm{E}[Z(\mathbf{x}_0)] = \sum_{K = \mathrm{A,B}} \mathrm{E}[Z(\mathbf{x}_0)|\mathbf{x}_0 \in K]P(\mathbf{x}_0 \in K) = \mathrm{E}[Z(\mathbf{x}_0)|\mathbf{x}_0 \in \mathrm{A}]P(\mathbf{x}_0 \in \mathrm{A}) + \mathrm{E}[Z(\mathbf{x}_0)|\mathbf{x}_0 \in \mathrm{B}]P(\mathbf{x}_0 \in \mathrm{B}). \tag{A2}$$

We implicitly assume that the probabilities P are constant (known) values, though they are actually estimated from the data.

The ordinary kriging predictor for $Z(\mathbf{x}_0)$ based on the data in stratum K is $\hat{Z}_K(\mathbf{x}_0)$, which is unbiased if $\mathbf{x}_0$ belongs to stratum K. An unconditional unbiased kriging predictor for $Z(\mathbf{x}_0)$ is given by:

$$\hat{Z}(\mathbf{x}_0) = \hat{Z}_\mathrm{A}(\mathbf{x}_0)P(\mathbf{x}_0 \in \mathrm{A}) + \hat{Z}_\mathrm{B}(\mathbf{x}_0)P(\mathbf{x}_0 \in \mathrm{B}). \tag{A3}$$

Kriging variance

The kriging variance $\sigma^2_K(\mathbf{x}_0)$ for $\hat{Z}_K(\mathbf{x}_0)$ ($\mathbf{x}_0 \in K$) is defined as:

$$\begin{aligned}\sigma^2_K(\mathbf{x}_0) &= \mathrm{E}[\{\hat{Z}(\mathbf{x}_0) - Z(\mathbf{x}_0)\}^2 | \mathbf{x}_0 \in K] \\ &= \mathrm{E}[\{\hat{Z}_\mathrm{A}(\mathbf{x}_0)P(\mathbf{x}_0 \in \mathrm{A}) + \hat{Z}_\mathrm{B}(\mathbf{x}_0)P(\mathbf{x}_0 \in \mathrm{B}) - Z(\mathbf{x}_0)\}^2 | \mathbf{x}_0 \in K].\end{aligned} \tag{A4}$$

The kriging variance $\sigma^2(\mathbf{x}_0)$ of the predictor $\hat{Z}(\mathbf{x}_0)$ is obtained after integrating out the conditioning on region K:

$$\begin{aligned}\sigma^2(\mathbf{x}_0) &= \mathrm{E}[\{\hat{Z}(\mathbf{x}_0) - Z(\mathbf{x}_0)\}^2] \\ &= \sum_{K = \mathrm{A,B}} \mathrm{E}[\{P(\mathbf{x}_0 \in \mathrm{A})\hat{Z}_\mathrm{A}(\mathbf{x}_0) + P(\mathbf{x}_0 \in \mathrm{B})\hat{Z}_\mathrm{B}(\mathbf{x}_0) - Z_K(\mathbf{x}_0)\}^2 | \mathbf{x}_0 \in K]P(\mathbf{x}_0 \in K) \\ &= \mathrm{E}[\{P(\mathbf{x}_0 \in \mathrm{A})(\hat{Z}_\mathrm{A}(\mathbf{x}_0) - Z_\mathrm{A}(\mathbf{x}_0)) + P(\mathbf{x}_0 \in \mathrm{B})(\hat{Z}_\mathrm{B}(\mathbf{x}_0) - Z_\mathrm{A}(\mathbf{x}_0))\}^2]P(\mathbf{x}_0 \in \mathrm{A}) \\ &\quad + \mathrm{E}[\{P(\mathbf{x}_0 \in \mathrm{A})(\hat{Z}_\mathrm{A}(\mathbf{x}_0) - Z_\mathrm{B}(\mathbf{x}_0)) + P(\mathbf{x}_0 \in \mathrm{B})(\hat{Z}_\mathrm{B}(\mathbf{x}_0) - Z_\mathrm{B}(\mathbf{x}_0))\}^2]P(\mathbf{x}_0 \in \mathrm{B}) \\ &= P(\mathbf{x}_0 \in \mathrm{A})^3\sigma^2_\mathrm{A}(\mathbf{x}_0) + P(\mathbf{x}_0 \in \mathrm{B})^3\sigma^2_\mathrm{B}(\mathbf{x}_0) \\ &\quad + 2\,P(\mathbf{x}_0 \in \mathrm{A})^2\,P(\mathbf{x}_0 \in \mathrm{B})\mathrm{E}[\{\hat{Z}_\mathrm{A}(\mathbf{x}_0) - Z_\mathrm{A}(\mathbf{x}_0)\}\{\hat{Z}_\mathrm{B}(\mathbf{x}_0) - Z_\mathrm{A}(\mathbf{x}_0)\}] \\ &\quad + 2\,P(\mathbf{x}_0 \in \mathrm{B})^2\,P(\mathbf{x}_0 \in \mathrm{A})\mathrm{E}[\{\hat{Z}_\mathrm{B}(\mathbf{x}_0) - Z_\mathrm{B}(\mathbf{x}_0)\}\{\hat{Z}_\mathrm{A}(\mathbf{x}_0) - Z_\mathrm{B}(\mathbf{x}_0)\}] \\ &\quad + P(\mathbf{x}_0 \in \mathrm{A})^2P(\mathbf{x}_0 \in \mathrm{B})\mathrm{E}[\{\hat{Z}_\mathrm{A}(\mathbf{x}_0) - Z_\mathrm{B}(\mathbf{x}_0)\}^2] \\ &\quad + P(\mathbf{x}_0 \in \mathrm{B})^2\,P(\mathbf{x}_0 \in \mathrm{A})\mathrm{E}[\{\hat{Z}_\mathrm{B}(\mathbf{x}_0) - Z_\mathrm{A}(\mathbf{x}_0)\}^2].\end{aligned} \tag{A5}$$

Covariances $\mathrm{Cov}\{\hat{Z}_\mathrm{A}(\mathbf{x}_0), \hat{Z}_\mathrm{B}(\mathbf{x}_0)\}$, $\mathrm{Cov}\{\hat{Z}_\mathrm{A}(\mathbf{x}_0), Z_\mathrm{B}(\mathbf{x}_0)\}$ and $\mathrm{Cov}\{\hat{Z}_\mathrm{B}(\mathbf{x}_0), Z_\mathrm{A}(\mathbf{x}_0)\}$ are considered zero by the conceptual design of the methodology. Using this and the condition that $P(\mathbf{x}_0 \in \mathrm{A}) + P(\mathbf{x}_0 \in \mathrm{B}) = 1$, Equation (A5) can be simplified:

$$\begin{aligned}\sigma^2(\mathbf{x}_0) = \sigma^2_\mathrm{A}(\mathbf{x}_0)P(\mathbf{x}_0 \in \mathrm{A})^2 + \sigma^2_\mathrm{B}(\mathbf{x}_0)P(\mathbf{x}_0 \in \mathrm{B})^2 + P(\mathbf{x}_0 \in \mathrm{A})P(\mathbf{x}_0 \in \mathrm{B}) \\ [\{\mathrm{E}[Z_\mathrm{A}(\mathbf{x}_0)] - \mathrm{E}[Z_\mathrm{B}(\mathbf{x}_0)]\}^2 + \mathrm{Var}\{Z_\mathrm{A}(\mathbf{x}_0)\} + \mathrm{Var}\{Z_\mathrm{B}(\mathbf{x}_0)\}],\end{aligned} \tag{A6}$$

where $\mathrm{Var}\{.\}$ is defined as $\mathrm{Var}\{Z_K(\mathbf{x}_0)\} = \mathrm{E}[\{Z_K(\mathbf{x}_0) - \mathrm{E}[Z_k(\mathbf{x}_0)]\}^2]$, which is equivalent to the sill of the variogram of stratum K. Equation (A6) is solved under the assumption that the kriging variances and the stratum means are known, whereas in reality these quantities must be estimated from the observations. The bias which may be introduced in this way is small because the number of observations is large, however. The kriging predictor for $\sigma^2(\mathbf{x}_0)$ is given by:

$$\hat{\sigma}^2(\mathbf{x}_0) = P(\mathbf{x}_0 \in \mathrm{A})^2\hat{\sigma}^2_\mathrm{A}(\mathbf{x}_0) + P(\mathbf{x}_0 \in \mathrm{B})^2\hat{\sigma}^2_\mathrm{B}(\mathbf{x}_0) + P(\mathbf{x}_0 \in \mathrm{A})P(\mathbf{x}_0 \in \mathrm{B})[\{\hat{z}_\mathrm{A}(\mathbf{x}_0) - \hat{z}_\mathrm{B}(\mathbf{x}_0)\}^2 + c_\mathrm{A} + c_\mathrm{B}], \qquad \forall \mathbf{x}_0 \in \mathrm{S}, \tag{A7}$$

where c_A and c_B are the sills of the variograms of the strata A and B.